Crystal Growth

International Edition: DOI: 10.1002/anie.201508763
German Edition: DOI: 10.1002/ange.201508763

In Situ Observation of Successive Crystallizations and Metastable Intermediates in the Formation of Metal–Organic Frameworks

Hamish H.-M. Yeung, Yue Wu, Sebastian Henke, Anthony K. Cheetham, Dermot O'Hare, and Richard I. Walton**

Abstract: *Understanding the driving forces controlling crystallization is essential for the efficient synthesis and design of new materials, particularly metal–organic frameworks (MOFs), where mild solvothermal synthesis often allows access to various phases from the same reagents. Using high-energy in situ synchrotron X-ray powder diffraction, we monitor the crystallization of lithium tartrate MOFs, observing the successive crystallization and dissolution of three competing phases in one reaction. By determining rate constants and activation energies, we fully quantify the reaction energy landscape, gaining important predictive power for the choice of reaction conditions. Different reaction rates are explained by the structural relationships between the products and the reactants; larger changes in conformation result in higher activation energies. The methods we demonstrate can easily be applied to other materials, opening the door to a greater understanding of crystallization in general.*

The formation mechanisms of crystalline materials from solution have long presented a challenge to researchers, owing to the multiple length scales involved in the crystallization process. Understanding the driving forces of crystallization can have several profound effects, for example in polymorph selection, yield, purity, and in defect control. In porous metal–organic frameworks (MOFs), which have applications ranging from gas storage[1–3] and catalysis[4,5] to separations,[6,7] crystallization depends on a delicate interplay between dissolution, monomer formation, aggregation, and formation of a bulk crystal lattice. Denser MOF systems have also come to the fore, exploiting the synergy between organic and inorganic components, which results in extreme flexibility,[8–13] multiferroic behavior,[14,15] ion dynamics,[16,17] and electronic conductivity.[18–20] However, no single technique can probe all of the length scales involved in crystallization and, furthermore, the difficulty in designing in situ experiments under the solvothermal conditions typical for MOFs has meant that only since 2006 have such studies been reported.[21–32] Of all the bulk in situ techniques used to study MOF formation to date, energy-dispersive diffraction of white-beam X-rays is perhaps the most developed, allowing quantitative information about both crystal nucleation and growth to be extracted from changes in the intensities of single diffraction peaks, providing their origin is established using other, ex situ methods.[26,27,29–31]

As important as crystallization kinetics are the underlying thermodynamics, which ultimately define the relative stability of competing reaction products. In MOFs, although different phases can crystallize from similar reagent mixtures, very little is known about the thermodynamic factors controlling their formation.[33–35] In an effort to understand the competing formation of different MOF phases, we and others reported structural analyses and first-principles calculations of 14 dense lithium tartrate MOFs with the formula $Li_{2-x}H_x(C_6H_4O_6)(H_2O)_y$.[36,37] Such large phase diversity enabled us to hypothesize that low-density structures, such as $Li_2(meso\text{-}C_6H_4O_6)(H_2O)_{0.5}$ (**1**) and $Li_2(meso\text{-}C_6H_4O_6)$ (**2a**) with *gauche* ligand conformation (the preferred conformation of *meso*-tartaric acid)[38] and chelation binding to Li, might be kinetic products, whereas the denser phase $Li_2(meso\text{-}C_6H_4O_6)$ (**2b**), which has monodentate binding, should be the thermodynamic product. Indeed, **2b** was shown by DFT calculations to be 7.59 kJ mol^{-1} lower in energy than **2a** despite its non-equilibrium *trans* ligand conformation, which might result in a higher activation barrier to its formation (Figure 1).[39,40] However, no study has yet been able to link fundamental thermodynamics of MOF formation with quantitative kinetics; even relative energies of reactants with respect to products remain undetermined.

To overcome the experimental challenges required to link thermodynamic insight with new kinetic parameters, we have performed in situ diffraction using high energy, monochromatic X-rays[41] to increase the detected range of *d* spacings beyond that obtainable with white-beam X-rays, enabling

[*] Dr. H. H.-M. Yeung
International Center for Materials Nanoarchitectonics (MANA)
National Institute for Materials Science
Namiki 1-1, Tsukuba, Ibaraki 305-0044 (Japan)
and
International Center for Young Scientists (ICYS)
National Institute for Materials Science
Sengen 1–2-1, Tsukuba, Ibaraki, 305-0047 (Japan)
E-mail: YEUNG.Hamishheiman@nims.go.jp
Dr. Y. Wu, Prof. Dr. D. O'Hare
Chemistry Research Laboratory, University of Oxford
Mansfield Road, Oxford, OX1 3TA (UK)
Dr. S. Henke
Lehrstuhl für Anorganische Chemie II, Ruhr-Universität Bochum
Universitätstrasse 150, 44801 Bochum (Germany)
Dr. S. Henke, Prof. Dr. A. K. Cheetham
Department of Materials Science and Metallurgy
Cambridge University
27 Charles Babbage Road, Cambridge, CB3 0FS (UK)
Prof. Dr. R. I. Walton
Department of Chemistry, University of Warwick
Coventry, CV4 7AL (UK)
E-mail: R.I.Walton@warwick.ac.uk

Supporting information and ORCID(s) from the author(s) for this article are available on the WWW under http://dx.doi.org/10.1002/anie.201508763.

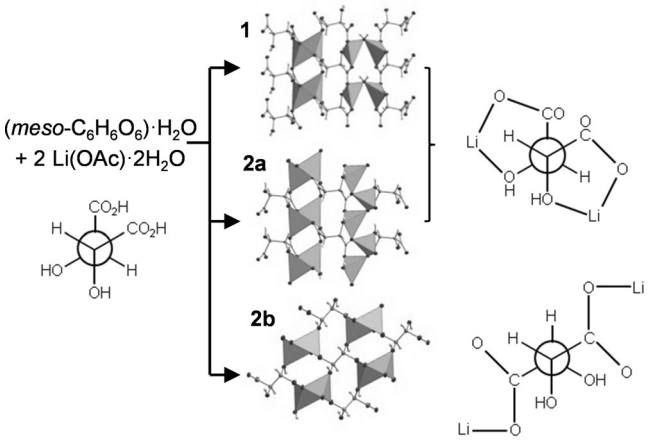

Figure 1. Possible products in the formation of lithium *meso*-tartrates, showing ligand conformations and major binding modes as a Newman projection.

phase identification directly from the in situ data. Reactions were performed in a large volume reactor, mimicking real laboratory conditions, between lithium acetate and *meso*-tartaric acid in water/ethanol at a series of temperatures between 40.1(4) and 123.6(3) °C (see Section S1 in the Supporting Information for details). Phase identification of the in situ X-ray diffraction patterns reveals that formation of the thermodynamic product **2b** is preceded by two phases: first by the hydrated analogue **1**, and subsequently by the metastable anhydrous polymorph **2a** (Figure 2; Figures S1–S7 in the Supporting Information). The progression of reaction products, which our evidence suggests occurs through dissolution and recrystallization rather than solid–solid transformations, corresponds to increasing density in the order **1**→**2a**→**2b**, in agreement with Ostwald's rule of stages.[42]

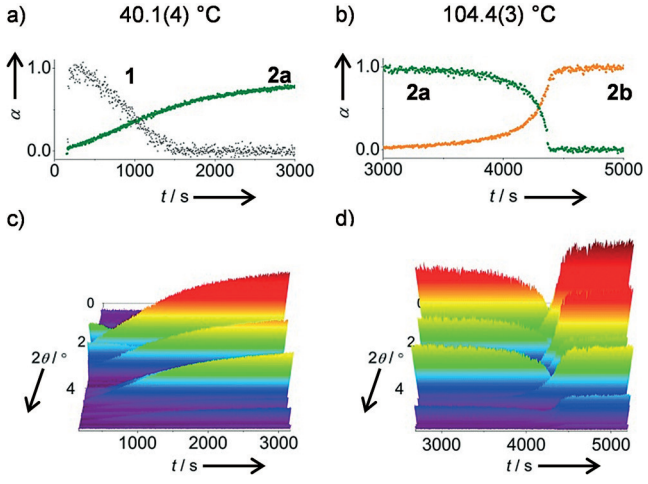

Figure 2. Solvothermal conversions between lithium tartrate MOFs, showing a, b) the extent of crystallization (α) as a function of reaction time (t). These data were extracted from c, d) in situ XRD data, where 2θ is the diffraction angle. a, c) Hydrated phase **1** (grey points) is converted into metastable phase **2a** (green points), followed by b, d) conversion of **2a** into the thermodynamic product **2b** (orange points). $\lambda = 0.2326$ Å.

After development of a new crystallization model to fit the changes in diffraction peak intensity (see the following section), the rate constants and exponents could be extracted for most nucleation, growth, and dissolution processes (Table 1). In general, the MOF formation reactions occur faster at higher temperatures, such that owing to the delay in data collection (150–180 s after the start of each reaction), the crystallization of **1** is missed entirely and the initial rise of **2a** is missed above 96.6(2) °C. For these cases, we can simply make the qualitative observations that nucleation occurs faster than could be measured by our experiment, giving the nucleation rate constant, $k_N(\mathbf{1})$, a minimum value of $11 \times 10^{-3}\ s^{-1}$ (conservatively assuming the time of peak nucleation (a_N) occurs midway between $t = 0$ and the start of data collection, 150–180 s).

Crystallization of **2a** was detected at all temperatures, and the changes in integrated peak intensities were fitted using the Avrami–Erofe'ev expression for crystal growth, $\alpha = G(t) = 1 - \exp(-(k_G t)^{n_G})$, where α is the extent of crystallization, $G(t)$ defines the crystal growth function, k_G is the crystal growth rate constant, t is the reaction time, and n_G is the crystal growth exponent.[43] Where the initial rise was observed such that the effect of nucleation, $N(t)$, could also be taken into account, intensities were fitted using the Gualtieri expression, $\alpha = N(t)G(t) = (1/(1 + \exp((t - a_N)/b_N)))G(t)$, where a_N is the reciprocal of the nucleation rate constant k_N, and b_N is the variance of the nucleation probability distribution (see Section S2, Table S1, and Figure S8 for detailed descriptions and fitted parameters).[44] Up to 104.4(3) °C, both $k_N(\mathbf{2a})$ and the crystal growth rate constant, $k_G(\mathbf{2a})$, increase with temperature, as expected for thermally activated processes. The crystal growth exponent, $n_G(\mathbf{2a})$, is consistently less than unity, indicating that growth is surface-reaction limited, rather than diffusion limited.[45] Unlike other MOF systems, for which n_G could be fixed at integer values suggestive of particle growth dimensionality,[26,27,31,46] it appears as if particle morphology plays no rate limiting role in the crystallization of the lithium *meso*-tartrates.

In the past, several equations, including power laws, have been used to model dissolution kinetics but with limited physical meaning ascribable to the fitted parameters.[27,47] Given that both **2a** and **2b** form and interconvert, even after the in situ heating, with below-quantitative yields (Table 1; Section S3), we may assume that lithium tartrate MOFs exist in dynamic equilibrium with dissolved precursors. It therefore seems reasonable to model the dissolution of **1** and **2a** as the time-reversed equivalent of crystal growth, that is, the Avrami–Erofe'ev equation $D(t) = G(t_{0,D} - t) = 1 - \exp(-(k_D(t_{0,D} - t))^{n_D})$, where k_D is the dissolution rate constant, n_G is the dissolution exponent, and $t_{0,D}$ marks the end of the dissolution process, after which all subsequent growth of the new phase must come from diffraction-invisible species, that is, monomeric species or dissolved nuclei. In this way, we can directly compare the rate constants and the exponents of crystallization and dissolution to provide meaningful insight into the reaction mechanisms of the different processes. Combining $D(t)$ with $G(t)$ in a single

Table 1: Phase identification for the formation of lithium *meso*-tartrates, showing reaction temperatures, rate constants, and exponents extracted from kinetic modelling of in situ X-ray diffraction data, plus final products and yields measured ex situ.

T	First phase[a,b]						Second phase[b,c]				Final phase[d]	
[°C]	ID	k_N [$\times10^{-3}$ s^{-1}]	k_G [$\times10^{-3}$ s^{-1}]	n_G	k_D [$\times10^{-3}$ s^{-1}]	n_D	ID	k_N [$\times10^{-3}$ s^{-1}]	k_G [$\times10^{-3}$ s^{-1}]	n_G	ID	Yield [%]
40.1(4)	**1**	–	–	–	0.93(7)	2.9(3)	**2a**	1.76(6)	0.574(7)	0.78(3)	**2a**	30
58(1)	**1**	–	–	–	11(3)	1.5(7)	**2a**	3.96(10)	2.43(13)	0.362(14)	**2b**	59
78(2)	**2a**	12.9(12)	3.25(7)	0.368(10)	–	–	–	–	–	–	**2b**	57
96.6(2)	**2a**	–	7.5(2)	0.291(7)	–	–	–	–	–	–	**2a**	39
104.4(3)	**2a**	–	12.3(7)	0.47(2)	7.25(13)	0.614(11)	**2b**	0.2262(3)	34.5(13)	0.577(14)	**2b**	66
111.0(4)	**2a**	–	8.9(5)	0.63(5)	10.4(3)	0.76(2)	**2b**	0.538(2)	210(40)	0.160(19)	**2b**	50
123.6(3)	**2a**	–	7.9(4)	0.73(4)	33.3(19)	0.50(2)	**2b**	0.3782(2)	430(140)	0.33(3)	**2b**	70

[a] Where the initial rise of the crystallization curve occurred before data collection, nucleation parameters were not extracted. [b] ID = identity of the phase, k_N = nucleation rate constant, k_G = crystal growth rate constant, n_G = crystal growth exponent, k_D = dissolution rate constant, n_D = dissolution exponent. [c] At 78(2) °C and 96.6(2) °C, **2a** remained stable for the duration of the in situ experiment. [d] At 58(1) °C and 96.6(2) °C, phase change from **2a** to **2b** occurred after the in situ experiment (see Section S3).

expression provides a good fit to the changes in integrated peak intensity over the course of the entire reaction for **1** and **2a** above 104.4(3) °C (see Table S2 and Figures S9–10). Values of $n_D(\mathbf{1}) = 2.9(3)$ and 1.5(7) suggest that dissolution of **1** is multidimensional, with a heavily temperature-dependent rate constant k_D. In contrast, $n_D(\mathbf{2a})$ is, like $n_G(\mathbf{2a})$, consistently below unity, suggesting that the same reaction mechanism may indeed be responsible for the dissolution of **2a** as for its growth.

Above 104.4(3) °C, the crystallization of the thermodynamic product **2b** was observed. Owing to severe asymmetry in the sigmoidal crystallization curves (that is, the long initial rise and short time to reach a plateau) neither Gualtieri nor Avrami–Erofe'ev crystallization models described the growth of **2b** adequately. Instead, we propose to split the two functions contained in the Gualtieri model into distinct sections separated by a refinable variable $t_{0,G}$. This variable gives an estimate of the cross-over between the nucleation-related regime, which should be dependent on the dissolution of **2a**, and the growth-related regime, which should be independent: for $t < t_{0,G}$,

$$\alpha = N(t) = (1/(1 + \exp((t - a_N)/b_N))),$$

and for $t \geq t_{0,G}$,

$$\alpha = G(t) = 1 - \exp(-(k_G(t_{0,G} - t))^{n_G}).$$

Despite the possibility of a discontinuity at $t = t_{0,G}$, the split Gualtieri model provides a much improved fit to both the extended nucleation process and the crystal growth process (see Tables S3–4 and Figures S11–12). Furthermore, since at each temperature $t_{0,G}(\mathbf{2b})$ lies close in time to $t_{0,D}(\mathbf{2a})$, we can be confident that the crystal growth parameters of **2b**, namely $k_G(\mathbf{2b})$ and $n_G(\mathbf{2b})$, are both independent of its nucleation kinetics and independent of the dissolution of **2a**.

In general, there is no reason why simple nucleation–growth models such as those of Gualtieri and Avrami–Erofe'ev should fit well when we are dealing with successive transformations; the growth of the second phase must relate to the decay of the first, as well as any diffraction-invisible species already in solution. After formation of phase **2a** the concentration of reactant is lower than the initial concentration, and so the initial rise of **2b** takes longer compared to **2a**. As **2b** forms, **2a** acts to maintain the amount of the reactant in solution by gradual redissolution. Only once **2a** has completely dissolved (i.e. $t > t_{0,D} \approx t_{0,G}$) does the crystallization curve of **2b** resemble conventional crystal growth, with the formation of a plateau in the crystallization curve a result of decreasing reactant concentration as it is used up to form **2b**.

Whilst $k_G(\mathbf{2b})$ increases with temperature, $k_N(\mathbf{2b})$ increases to 111.0(4) °C, then decreases at 123.6(3) °C. We believe this may be because of the increasing importance of entropy at high temperatures, which is known to stabilize low-density, metastable polymorphs.[39,48] This results in higher yields of **2a** and therefore a lower concentration of reagent remaining in solution, further inhibiting the nucleation of **2b**. Similarly, $k_G(\mathbf{2a})$ decreases slightly above 104.4(3) °C, a likely effect of lower reactant concentrations induced by the competing crystallization of **2b**. The fact that $k_G(\mathbf{2b})$ is always several orders of magnitude larger than $k_G(\mathbf{2a})$ is a reflection of the larger overall driving force to form the thermodynamic product from the starting materials.

Activation energies were calculated by using Arrhenius plots of the rate constant data (Figure S13, Table S5). The activation energies for nucleation ($E_{A,N}(\mathbf{2a})$) and crystal growth ($E_{A,G}(\mathbf{2a})$) have similar values, 51(6) kJ mol^{-1} and 41(3) kJ mol^{-1}, respectively, suggesting the same rate-determining process for both. We hypothesize that the ligand–metal interactions with the necessary conformations for crystallization of **2a** and **2b** are generated through reactions at the growing crystal surfaces, as suggested by the low values of $n_G(\mathbf{2a})$ and $n_G(\mathbf{2b})$. These activation energies are lower than those of prototypical MOFs, HKUST-1 ($E_{A,N}$ = 71.6 kJ mol^{-1}) and MOF-14 ($E_{A,N}$ = 113.9 kJ mol^{-1}),[27] indicative of the lability of the Li coordination sphere compared to transition metals such as Zn and Cu which are commonly used in porous MOFs. In contrast, $E_{A,G}(\mathbf{2b})$ is around four times higher at 210(80) kJ mol^{-1}, indicative of the unfavorable change in ligand conformation necessary for the formation of **2b**. The activation energy for dissolution of **2a**, $E_{A,D}(\mathbf{2a})$, is 90(20) kJ mol^{-1}. To our knowledge, this is the first time that activation energies for both crystal growth and dissolution of one phase have been obtained from a single experiment. Importantly, this enables us to calculate a thermodynamic

quantity from kinetic parameters without the need for expensive computation or calorimetry. Subtracting $E_{A,G}$(**2a**) from $E_{A,D}$(**2a**) gives the energy difference between solvated reactants and **2a**: ΔE_{rel}(reactants−**2a**) = 50(20) kJ mol^{-1}.

Knowledge of the activation energies allows us to formally quantify the relationship between formation kinetics and thermodynamic stability of the lithium *meso*-tartrates for the first time. Figure 3 shows the reaction energy profile of the conversion of solvated reagents—lithium acetate and tartaric acid—into the MOF phases **1**, **2a**, and **2b**. Relative energies of each phase are shown by the horizontal lines. The heights of the curves correspond to activation energies of crystal growth ($E_{A,G}$) and dissolution ($E_{A,D}$), quantifying the energetics of the structural changes (for example, ligand conformation, metal binding modes)[39] needed to form each phase. It can be seen that as thermodynamic stability increases, so does the activation energy for the formation reaction.

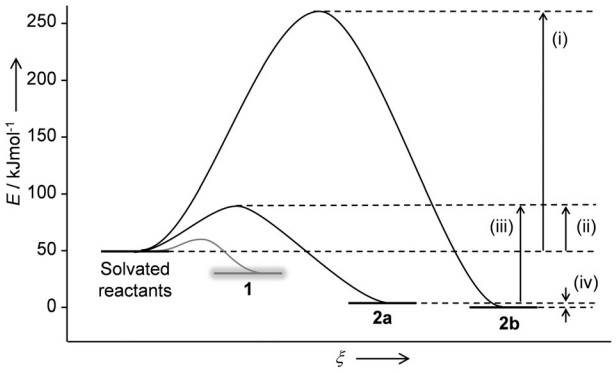

Figure 3. Reaction energy profile (relative to phase **2b**) plotting energy (E) against reaction progress (ξ) for the formation of lithium *meso*-tartrate MOFs. The profile shows experimentally determined activation energies i) $E_{A,G}$(**2b**) = 210(80) kJ mol^{-1}, ii) $E_{A,G}$(**2a**) = 41(3) kJ mol^{-1}, iii) $E_{A,D}$(**2a**) = 90(20) kJ mol^{-1}, and thermodynamic stability calculated by DFT[37] iv) ΔE_{rel}(**2a**–**2b**) = 7.59 kJ mol^{-1}. The energy profile of **1**, currently undetermined, is shown qualitatively for comparison.

In summary, we have been able to quantify the energetics of the crystallization of a family of MOFs in terms of both kinetic and thermodynamic factors. The increased angular resolution obtained with high-energy, monochromatic X-rays allows separation of the Bragg peaks of materials with low-symmetry structures to an extent not possible with previously used energy-dispersive X-ray methods. Thus, using our setup we have been able to identify the temperature-dependent crystallization and interconversion of three different lithium *meso*-tartrate phases, enabling the determination of rate constants and activation energies for nucleation, growth, and dissolution by fitting two new kinetic models to the changes in peak intensity with time. The thermodynamically most stable phase **2b** forms via successive intermediates, **1** and **2a**, and requires a substantially larger activation energy to be overcome for its formation (210(80) kJ mol^{-1} versus 41(3) kJ mol^{-1} for **2a**) owing to the unfavorable change in ligand conformation (note that this is in the opposite sense to the Brønsted–Evans–Polanyi principle[49]). This suggests that changes in ligand conformation might play a rate-limiting role in the formation of MOFs with flexible ligands, even when transition metals are used. In this system, the differences in crystallization rates enable isolation of metastable **2a** (calculated to be just 7.59 kJ mol^{-1} higher in energy than **2b**)[37] but not **1**, which is only fleetingly apparent at the lowest temperatures. In addition, our ability to extract kinetic activation energies for both crystallization and dissolution of **2a** from one experiment has enabled us to calculate the relative thermodynamic stability of the products with respect to the reactants. To the best of our knowledge, this work provides the most comprehensive understanding of the energetics of MOF formation to date and yields improved experimental and analytical methods for the study of the synthesis and stability of crystalline materials in general.

Acknowledgements

We thank the Diamond Light Source for beamtime (beamline I12, reference EE9661) and Christina Reinhard for assistance, Andrew Jupe for providing FitChi and XYBruck programs, and Tadashi Ozawa and Kiyotaka Iiyama for assistance with microscopy. H.H.M.Y. acknowledges support from the World Premier International Research Center Initiative on Materials Nanoarchitectonics (WPI-MANA) from MEXT, Japan, and the Royal Society of Chemistry Journal Grants for International Authors for travel. S.H. acknowledges the Alexander von Humboldt Foundation for a Feodor Lynen Fellowship. Y.W. acknowledges the EU Seventh Framework Programme (grant agreement no. FP7-NMP4-LA-2012-280983, SHYMAN).

Keywords: crystal growth · metal–organic frameworks · metastable compounds · reaction kinetics · X-ray diffraction

How to cite: *Angew. Chem. Int. Ed.* **2016**, *55*, 2012–2016
Angew. Chem. **2016**, *128*, 2052–2056

[1] L. J. Murray, M. Dincă, J. R. Long, *Chem. Soc. Rev.* **2009**, *38*, 1294–1314.
[2] J.-R. Li, R. J. Kuppler, H.-C. Zhou, *Chem. Soc. Rev.* **2009**, *38*, 1477–1504.
[3] D. J. Tranchemontagne, K. S. Park, H. Furukawa, J. Eckert, C. B. Knobler, O. M. Yaghi, *J. Phys. Chem. C* **2012**, *116*, 13143–13151.
[4] J. Lee, O. K. Farha, J. Roberts, K. A. Scheidt, S. T. Nguyen, J. T. Hupp, *Chem. Soc. Rev.* **2009**, *38*, 1450–1459.
[5] L. Ma, C. Abney, W. Lin, *Chem. Soc. Rev.* **2009**, *38*, 1248–1256.
[6] A. Comotti, S. Bracco, P. Sozzani, S. Horike, R. Matsuda, J. Chen, M. Takata, Y. Kubota, S. Kitagawa, *J. Am. Chem. Soc.* **2008**, *130*, 13664–13672.
[7] J.-R. Li, J. Sculley, H.-C. Zhou, *Chem. Rev.* **2012**, *112*, 869–932.
[8] G. Férey, C. Serre, *Chem. Soc. Rev.* **2009**, *38*, 1380–1399.
[9] S. Horike, S. Shimomura, S. Kitagawa, *Nat. Chem.* **2009**, *1*, 695–704.
[10] S. Henke, A. Schneemann, R. A. Fischer, *Adv. Funct. Mater.* **2013**, *23*, 5990–5996.
[11] A. Schneemann, V. Bon, I. Schwedler, I. Senkovska, S. Kaskel, R. A. Fischer, *Chem. Soc. Rev.* **2014**, *43*, 6062–6096.
[12] W. Cai, A. Katrusiak, *Nat. Commun.* **2014**, *5*, 4337.
[13] M. T. Wharmby, S. Henke, T. D. Bennett, S. R. Bajpe, I. Schwedler, S. P. Thompson, F. Gozzo, P. Simoncic, C. Mellot-

Draznieks, H. Tao, Y. Yue, A. K. Cheetham, *Angew. Chem. Int. Ed.* **2015**, *54*, 6447 – 6451; *Angew. Chem.* **2015**, *127*, 6547 – 6551.
[14] P. Jain, V. Ramachandran, R. J. Clark, H. D. Zhou, B. H. Toby, N. S. Dalal, H. W. Kroto, A. K. Cheetham, *J. Am. Chem. Soc.* **2009**, *131*, 13625 – 13627.
[15] D.-W. Fu, W. Zhang, H.-L. Cai, Y. Zhang, J.-Z. Ge, R.-G. Xiong, S. D. Huang, T. Nakamura, *Angew. Chem. Int. Ed.* **2011**, *50*, 11947 – 11951; *Angew. Chem.* **2011**, *123*, 12153 – 12157.
[16] S. Horike, D. Umeyama, S. Kitagawa, *Acc. Chem. Res.* **2013**, *46*, 2376 – 2384.
[17] S. Tominaka, S. Henke, A. K. Cheetham, *CrystEngComm* **2013**, *15*, 9400 – 9407.
[18] A. A. Talin, A. Centrone, A. C. Ford, M. E. Foster, V. Stavila, P. Haney, R. A. Kinney, V. Szalai, F. El Gabaly, H. P. Yoon, F. Léonard, M. D. Allendorf, *Science* **2014**, *343*, 66 – 69.
[19] D. Sheberla, L. Sun, M. A. Blood-Forsythe, S. Er, C. R. Wade, C. K. Brozek, A. Aspuru-Guzik, M. Dincă, *J. Am. Chem. Soc.* **2014**, *136*, 8859 – 8862.
[20] S. Tominaka, H. Hamoudi, T. Suga, T. D. Bennett, A. B. Cairns, A. K. Cheetham, *Chem. Sci.* **2015**, *6*, 1465 – 1473.
[21] S. Surblé, F. Millange, C. Serre, G. Férey, R. I. Walton, *Chem. Commun.* **2006**, 1518 – 1520.
[22] S. Hermes, T. Witte, T. Hikov, D. Zacher, S. Bahnmüller, G. Langstein, K. Huber, R. A. Fischer, *J. Am. Chem. Soc.* **2007**, *129*, 5324 – 5325.
[23] M. Shöâeè, J. R. Agger, M. W. Anderson, M. P. Attfield, *CrystEngComm* **2008**, *10*, 646 – 648.
[24] D. Zacher, J. Liu, K. Huber, R. A. Fischer, *Chem. Commun.* **2009**, 1031 – 1033.
[25] J. Cravillon, S. Münzer, S. J. Lohmeier, A. Feldhoff, K. Huber, M. Wiebcke, *Chem. Mater.* **2009**, *21*, 1410 – 1412.
[26] F. Millange, M. I. Medina, N. Guillou, G. Férey, K. M. Golden, R. I. Walton, *Angew. Chem. Int. Ed.* **2010**, *49*, 763 – 766; *Angew. Chem.* **2010**, *122*, 775 – 778.
[27] F. Millange, R. El Osta, M. E. Medina, R. I. Walton, *CrystEngComm* **2011**, *13*, 103 – 108.
[28] J. Cravillon, R. Nayuk, S. Springer, A. Feldhoff, K. Huber, M. Wiebcke, *Chem. Mater.* **2011**, *23*, 2130 – 2141.
[29] T. Ahnfeldt, N. Stock, *CrystEngComm* **2012**, *14*, 505 – 511.
[30] H. Reinsch, N. Stock, *CrystEngComm* **2012**, *15*, 544 – 550.
[31] R. El Osta, M. Feyand, N. Stock, F. Millange, R. I. Walton, *Powder Diffr.* **2013**, *28*, S256 – S275.
[32] M. Goesten, E. Stavitski, E. A. Pidko, C. Gücüyener, B. Boshuizen, S. N. Ehrlich, E. J. M. Hensen, F. Kapteijn, J. Gascon, *Chem. Eur. J.* **2013**, *19*, 7809 – 7816.
[33] L. N. Appelhans, M. Kosa, A. V. Radha, P. Simoncic, A. Navrotsky, M. Parrinello, A. K. Cheetham, *J. Am. Chem. Soc.* **2009**, *131*, 15375 – 15386.
[34] R. Galvelis, B. Slater, A. K. Cheetham, C. Mellot-Draznieks, *CrystEngComm* **2012**, *14*, 374 – 378.
[35] J. T. Hughes, T. D. Bennett, A. K. Cheetham, A. Navrotsky, *J. Am. Chem. Soc.* **2013**, *135*, 598 – 601.
[36] H. H.-M. Yeung, M. Kosa, M. Parrinello, P. M. Forster, A. K. Cheetham, *Cryst. Growth Des.* **2011**, *11*, 221 – 230.
[37] H. H.-M. Yeung, M. Kosa, M. Parrinello, A. K. Cheetham, *Cryst. Growth Des.* **2013**, *13*, 3705 – 3715.
[38] A. Janiak, U. Rychlewska, M. Kwit, U. Stępień, K. Gawrońska, J. Gawroński, *ChemPhysChem* **2012**, *13*, 1500 – 1506.
[39] H. H.-M. Yeung, A. K. Cheetham, *Dalton Trans.* **2014**, *43*, 95 – 102.
[40] For ease of cross-referencing, the phase numbers used in this paper, **1**, **2a**, and **2b**, correspond to phases **11**, **7**, and **6**, respectively, in Ref. [39] and also to CCDC 944908, 960420, and 960419. CCDC data can be obtained free of charge from The Cambridge Crystallographic Data Centre. See Section S5 in the Supporting Information for more details.
[41] M. Drakopoulos, T. Connolley, C. Reinhard, R. Atwood, O. Magdysyuk, N. Vo, M. Hart, L. Connor, B. Humphreys, G. Howell, S. Davies, T. Hill, G. Wilkin, U. Pedersen, A. Foster, N. De Maio, M. Basham, F. Yuan, K. Wanelik, *J. Synchrotron Radiat.* **2015**, *22*, 828 – 838.
[42] W. Ostwald, *Z. Phys. Chem.* **1897**, *22*, 289 – 330.
[43] R. I. Walton, D. O'Hare, *J. Phys. Chem. B* **2001**, *105*, 91 – 96.
[44] A. F. Gualtieri, *Phys. Chem. Miner.* **2001**, *28*, 719 – 728.
[45] R. Viswanatha, D. D. Sarma, *Growth of Nanocrystals in Solution*, Wiley-VCH, Weinheim, **2007**.
[46] R. El Osta, M. Frigoli, J. Marrot, M. E. Medina, R. I. Walton, F. Millange, *Cryst. Growth Des.* **2012**, *12*, 1531 – 1537.
[47] P. J. Skrdla, *J. Pharm. Biomed. Anal.* **2007**, *45*, 251 – 256.
[48] G. Kieslich, S. Kumagai, K. T. Butler, T. Okamura, C. H. Hendon, S. Sun, M. Yamashita, A. Walsh, A. K. Cheetham, *Chem. Commun.* **2015**, *51*, 15538 – 15541.
[49] M. Polanyi, M. G. Evans, *Trans. Faraday Soc.* **1936**, *32*, 1333 – 1360.

Received: September 18, 2015
Revised: November 30, 2015
Published online: January 6, 2016

